On floating equilibria in a laterally finite container

John McCuan*and Ray Treinen†

August 8, 2016

Abstract

The main contribution of this paper is the precise numerical identification of a model set of parameters for a floating object/container system which admits three distinct equilibrium configurations, two of which are local energy minimizers among pseudo-equilibrium configurations. This numerical result strongly suggests the existence of a physical system in which an object can be observed to float in a centrally symmetric position in two geometrically distinct configurations, i.e., at two different heights. The numerical calculation relies on a fairly involved theoretical framework which can also be used to show uniqueness of equilibrium configurations for other parameters. Thus, the general dependence of observable stable equilibria on the physical parameters of the problem is both shown to be much more complicated than originally anticipated and likely to depend on additional information, e.g., the initial positioning of the floating object. In addition to providing a basis for numerical results, the theoretical framework developed here leads to two rigorous general results. The first is the existence of at least one equilibrium configuration when the density of the floating object is less than that of the liquid bath. The second is that all such equilibrium interfaces must project simply onto the base of the container.

Keywords. Floating objects, capillarity

Mathematics subject classification. 76B45

1 Introduction

Archimedes gave, perhaps, the earliest quantitatively precise model description of a physical system in which an object is deposited into a liquid bath (and either floats or sinks to the bottom). For a convex object which is not neutrally buoyant with respect to the liquid, Archimedes' model determines a unique floating (or sinking) configuration depending only on the ratio of the physical density of the object to that of the liquid.

Various scientists have observed the floating of objects with density greater than the density of the liquid bath into which they are deposited. That this can happen with a spherical object was demonstrated in [McC09] and/or [MT13] and also see [McC07]. Bhatnagar and Finn [BF06]

*School of Mathematics, Georgia Institute of Technology, 686 Cherry Street, Atlanta, GA 30332 (mccuan@math.gatech.edu).

†Department of Mathematics, Texas State University, 601 University Drive, San Marcos, Texas 78666 (rt30@txstate.edu).

seem to have been the first to prove such a situation arises in an idealized two-dimensional model involving an unbounded liquid bath, but also taking account of the effects of surface tension and wetting energy. The theoretical results of [MT13] show that a similar situation prevails in two and three-dimensional models and with laterally bounded containers. These results are in contradiction to Archimedes' assertions. While Archimedes' theory predicts that such an object sinks to the bottom, these latter results, which take account of surface tension and wetting energy, not only include a stable equilibrium with the object at the bottom, but they also feature an additional stable equilibrium with the object protruding above the liquid of the bath.

We also showed in [MT13] that at least two equilibria can be expected, one a local minimum for energy and another a local maximum among a one parameter family of pseudo-equilibria, which will be defined below. Numerical calculations described in [Tre16] also suggested that this situation prevails with some generality as the physical parameters are varied.

We emphasize that most of the work described above focused on the case of an object with density greater than that of the liquid and the analysis of how and why such an object can float at all. In this paper we focus on the complementary case where the density of the object is less than the density of the liquid and floating upon the surface of the liquid is very much to be expected. We anticipated that the situation would be somewhat similar, or perhaps simpler in some cases where it might be possible to show the uniqueness of a single equilibrium (minimum). In fact, the recent thesis of Hanzhe Chen [Che16] shows there can be at most two equilibria in the two-dimensional case with an unbounded bath. Much to our surprise, even in the simplest two-dimensional case (neglecting wetting energy) with a laterally bounded container, there can apparently be three distinct equilibrium configurations with two of them local minima among the pseudo-equilibria. We now describe such an example, amidst a general framework.

An equilibrium configuration for a circular object floating symmetrically in a laterally bounded container is indicated in Figure 1. The object (or its cross-section) is modeled by

$$\mathcal{B} = \overline{B_a(0,d)} = \{(x,z) \in \mathbb{R}^2 : x^2 + (z-d)^2 \leq a^2\}$$

where $a > 0$ is given and $d > 0$ is to be determined. The configuration includes an interface $\mathcal{S}$ consisting of two curves symmetric with respect to $x = 0$. Equilibrium configurations are critical for the functional

$$\mathcal{E} = \sigma \text{Length}(\mathcal{S}) - \sigma\beta \text{Length}(\mathcal{W}) - \sigma\beta_w \text{Length}(\mathcal{W}_w) + \int_{\mathcal{A}} \rho_\ell g z + \int_{\mathcal{B}} \rho g z$$

subject to the constraint

$$\text{Area}(\mathcal{A}) = A$$

where $\sigma > 0$ is a (surface) tension, $\beta = \beta_b$ and β_w are adhesion coefficients associated with the ball and the wall respectively, $\mathcal{W} = \mathcal{W}_b$ and $\mathcal{W}_w$ are the "wetted" portions of $\mathcal{B}$ and the container, $\rho = \rho_b$ and ρ_ℓ are densities in $\mathcal{B}$ and $\mathcal{A}$ respectively, and g is a gravitational constant. The problem may be interpreted to model an infinite log floating in an infinite trough or a long thin needle floating similarly on a liquid surface. Similar configurations for a floating circular object in a laterally infinite bath have been considered in a series of papers [BF06, Fin08, Fin10, Fin09, Fin11, FV09a, FV09b, FS09] of Finn and his coauthors as well as in a paper by Kemp and Siegel [KS11]. The significant complication introduced here is the presence of the laterally finite container and the associated volume constraint.

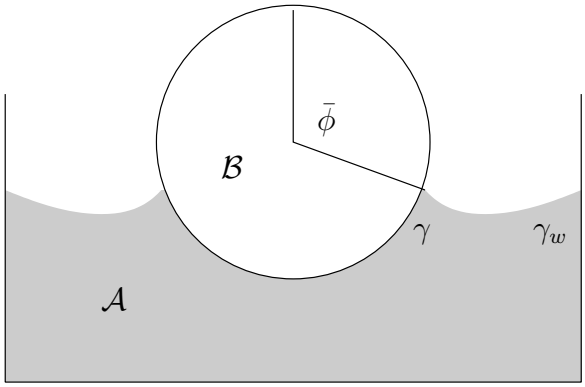

Figure 1: Floating circular object with azimuthal angle determined by triple contact point.

Our container is assumed to be determined by two "walls" at $x = \pm R$ with $R > a$ and a "floor" at $z = 0$, and it is assumed to contain enough liquid so that $\mathcal{B}$ may float without hitting the bottom.

In [MT13] we introduced the azimuthal angle $\bar{\phi}$ to describe the location of the contact point on the ball and gave the following necessary conditions for equilibrium:

- The curvature k of $\mathcal{S}$ is an affine function of the vertical position on the interface

  $$k = \kappa z - \lambda$$

  where $\kappa = \rho_\ell g/\sigma$ is the capillary constant.

- The interface meets the floating object at an angle satisfying $\cos\gamma = \beta$.

- The interface meets the wall at an angle satisfying $\cos\gamma_w = \beta_w$.

- The remaining parameters must satisfy the relation

  $$2\bar{\phi} + \sin(2\bar{\phi}) + \frac{4}{\kappa a^2}\sin(\bar{\phi} - \gamma) + \frac{4}{\kappa a}(\kappa d - \lambda)\sin\bar{\phi} = 2\pi\left(1 - \frac{\rho}{\rho_\ell}\right), \tag{1}$$

  which expresses a balance of buoyancy/pressure, weight, and capillary forces.

A configuration satisfying the first three conditions is called a *pseudo-equilibrium*. It is significant that the outer contact angle γ_w and the volume constraint appears only implicitly in the fourth condition through the unknowns λ and d. Some consequences of this observation will be important for us below. We turn our attention to the case $0 < \rho < \rho_\ell$ and prove the following result.

Theorem 1 *If $0 < \rho < \rho_\ell$ (and A large enough) there exists at least one equilibrium configuration satisfying the four necessary conditions listed above.*

2 Approach

In the discussion below we consider κ, a, R, A, γ, γ_w, and ρ/ρ_ℓ fixed and given. The problem then reduces to finding the unknowns $\bar{\phi}$, d and λ where $\bar{\phi} \in [0, \pi]$ is the azimuthal angle determining the contact point $(a \sin\bar{\phi}, d + a\cos\bar{\phi})$ at which the right interface meets the right half of the surface of $\mathcal{B}$. The volume constraint becomes

$$A = 2\left[\sin\bar{\phi}\left(d - \frac{\lambda}{\kappa} + \frac{1}{2}\cos\bar{\phi}\right) + \frac{1}{\kappa}\left(\cos\gamma_w - \sin(\gamma - \bar{\phi}) + \lambda R\right)\right] + \bar{\phi} - \pi.$$

Using this relation, λ may be expressed in terms of the two unknowns $\bar{\phi}$ and d, or d may be expressed in terms of λ and $\bar{\phi}$ as long as $\sin\bar{\phi} \neq 0$. In principle our treatment includes the extremal cases when $\bar{\phi} = 0, \pi$, though these two possibilities sometimes involve additional details and especially limits as $\bar{\phi}$ tends to the endpoints of the interval $(0, \pi)$. We have generally omitted these straightforward details.

In the sequel, we focus on the initial inclination angle $\theta = \gamma - \bar{\phi}$ of the interface where it meets $\partial\mathcal{B}$. It was observed in [MT13] that the force balance condition (1) may be rewritten as

$$2\bar{\phi} - \sin(2\bar{\phi}) + \frac{4}{\kappa a^2}\sin(\bar{\phi} - \gamma) + \frac{4\bar{k}}{\kappa a}\sin\bar{\phi} = 2\pi\left(1 - \frac{\rho}{\rho_\ell}\right), \tag{2}$$

where $\bar{k}$ is the curvature of the interface at the contact point. (Notice, when comparing (1) with (2), that the second term has changed sign.) Here we observe that if the value of $\bar{k}$ can be determined directly, along with $\bar{\phi}$, then we have a second relation $\bar{k} = \kappa(d + a\cos\bar{\phi}) - \lambda$ from which either d or λ may be determined.

In this way, our problem is effectively reduced to determining the values of $\bar{k}$ and $\bar{\phi}$ or, equivalently, the values of θ and $\zeta = \bar{k}/\kappa$ the normalized starting height for a geometric initial value problem we now describe.

3 Solution families

In order to organize the possible equilibrium interfaces, we temporarily forget about the relation $\theta = \gamma - \bar{\phi}$ and simply consider $\theta \in [-\pi, \pi]$ fixed. We also shift coordinates horizontally so that the right contact point $(a\sin\bar{\phi}, d + a\cos\bar{\phi})$ is taken to have first coordinate $x = 0$. We shift vertically, furthermore, so the Euler-Lagrange equation becomes

$$k = \kappa z.$$

As a consequence, we may assume the right portion of $\mathcal{S}$ is determined (up to a translation) as a solution of the initial value problem

$$\begin{cases} \dot{x} = \cos\psi, & x(0) = 0 \\ \dot{z} = \sin\psi, & z(0) = \zeta \\ \dot{\psi} = \kappa z, & \psi(0) = \theta. \end{cases} \tag{3}$$

Solutions of this problem are known to be defined for all $s > 0$ and are real analytic in the independent parameter s, which denotes arclength along the parameterized curve $(x(s), z(s))$. Solutions to the

problem also depend real analytically on the initial inclination angle θ and the initial starting height ζ. We will use a semicolon to indicate the secondary dependence on the initial values: $x = x(s) = x(s;\theta,\zeta)$.

Every solution of (3) can be identified by a point (θ,ζ,s_*) with (θ,ζ) in the phase plane for the decoupled system involving z and ψ which is indicated in Figure 2. The value $s_* > 0$ specifies

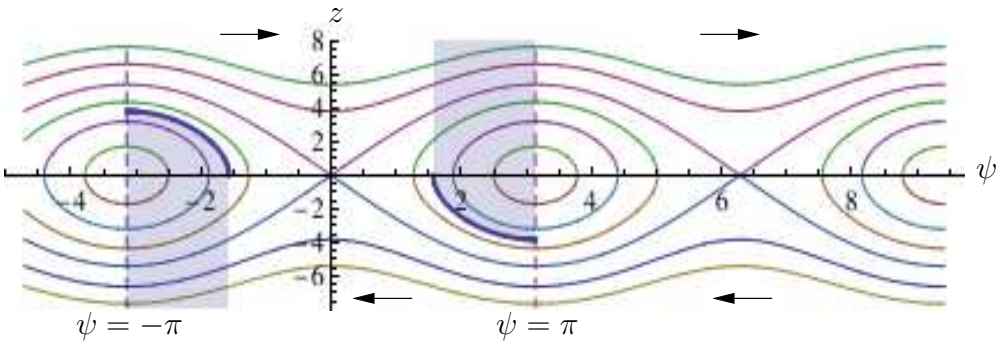

Figure 2: The phase plane for ψ and z. The shaded regions are bounded by portions of the curves $\pm z_{\pi/2} = \pm\sqrt{-2\cos\psi/\kappa}$ on which the conserved quantity takes the value 0 and represent initial values which will be shown inadmissible below. The flow along the level curves of $h = \kappa z^2/2 + \cos\psi$ is to the right for $z > 0$ and to the left for $z < 0$.

a particular domain $[0, s_*]$ upon which we consider the solution. The flow lines in Figure 2 are determined by the Hamiltonian/conserved quantity

$$h(\psi, z) = \frac{\kappa z^2}{2} + \cos\psi. \tag{4}$$

In order to organize the solutions appropriate to model interfaces as indicated in Figure 1, we impose the following conditions on the solutions we consider:

1. The *geometric interface curve* parameterized by

$$\alpha(s) = (x(s), z(s)), \qquad 0 \le s \le s_*$$

is an *embedded* curve.

2. The interface meets the closed right half of $\partial\mathcal{B}$ at $x(0) = 0$. Accordingly, we may assume

$$-\pi \le \theta \le \pi.$$

In fact, since $\theta = \gamma - \bar{\phi}$, we have the stricter condition

$$\gamma - \pi \le \theta \le \gamma, \tag{5}$$

though this involves $\bar{\phi}$ which will be suppressed in our initial analysis.

3. The interface is contained on the right:

$$x(s_*) > 0 \qquad \text{and} \qquad x(s) < x(s_*), \quad 0 \le s < s_*.$$

The condition $x(s) \le x(s_*)$, $s \in (0, s_*)$ implies there is some $k \in \mathbb{Z}$ such that $-\pi/2 \le \psi(s_*) + 2\pi k \le \pi/2$. The next condition requires that the integer $k = 0$.

4. The interface meets the right wall with the appropriate orientation:

$$-\pi/2 \le \psi(s_*) \le \pi/2.$$

This rules out configurations like that indicated in Figure 3(left).

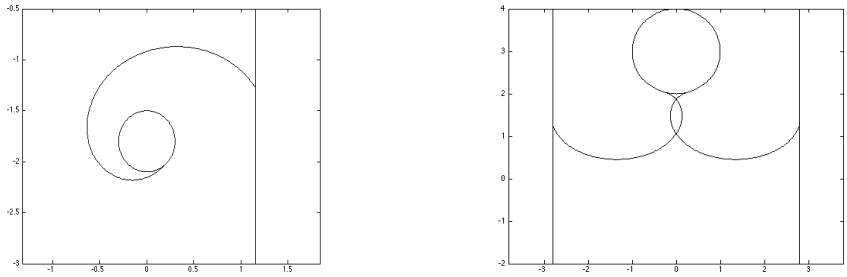

Figure 3: Formal interfaces which are non-physical. The interface on the left is not oriented correctly to contain a volume of liquid extending from the ball to the floor of the container. The interface on the right has two components which are not globally embedded.

We give an initial analysis of solutions based on these four conditions in Section 4 and denote the collection of all solutions satisfying them by $\mathcal{S}_0$. A secondary analysis in Section 6 is based on the next three conditions which take explicit account of the azimuthal angle $\bar{\phi}$ and the contact angles γ and γ_w.

5. The interface meets the right wall at the appropriate distance to the right:

$$x(s_*) = r = R - a \sin \bar{\phi}.$$

6. The interface meets the right wall at the correct angle:

$$\psi(s_*) = \pi/2 - \gamma_w.$$

7. Solutions do not extend to the left past the center of $\mathcal{B}$:

$$x(s) > -a \sin \bar{\phi}, \quad 0 < s \le s_*.$$

This condition rules out interfaces like that shown in Figure 3(right).

4 Initial classification of solutions

We seek to separate the phase plane into the projection of an initial potential solution set

$$\mathcal{S}_0 = \{(\theta, \zeta, s_*) : \text{conditions } 1-4 \text{ hold}\}$$

and a complementary region corresponding to excluded solutions. We begin by excluding certain regions of the phase plane.

First note that the periodic orbit passing through $(-\pi/2, 0)$ is a portion of the level curve $h(\psi, z) = 0$. Consequently, if $-\pi \le \theta \le -\pi/2$ and $\zeta < \sqrt{-2\cos\theta/\kappa}$, then it is readily verified that $\psi(s) < -\pi/2$ for all $s > 0$, and condition 4 cannot be satisfied. The borderline case $\zeta = \sqrt{-2\cos\theta/\kappa}$ can also be excluded since $x(s) \le 0$ whenever $\psi(s) = -\pi/2$ in violation of the combination of conditions 3 and 4. Similar considerations apply to a symmetric region with $\pi/2 \le \theta \le \pi$. Thus, we exclude

$$\left\{(\theta, \zeta) : \pi/2 \le |\theta| \le \pi,\ \operatorname{sign}(\theta)\zeta \ge -\sqrt{-2\cos\theta/\kappa}\right\}$$

as indicated in Figure 2.

Returning to $\theta \in (-\pi, -\pi/2)$, let us set $z_{\pi/2} := \sqrt{-2\cos\theta/\kappa}$ and consider $\zeta \in (z_{\pi/2}, \sqrt{2(1-\cos\theta)/\kappa})$. Note that $\zeta = z_\infty := \sqrt{2(1-\cos\theta)/\kappa}$ corresponds to the singular solution with $h(\psi, z) = 1$ indicated in Figure 6. Each corresponding solution of (3) with $z_{\pi/2} < \zeta < z_\infty$ will have

1. a first vertical point at some $s_a > 0$,
2. a first inflection at some $s_b > s_a$, and
3. a second vertical point at some (unique) $s_c > s_b$.

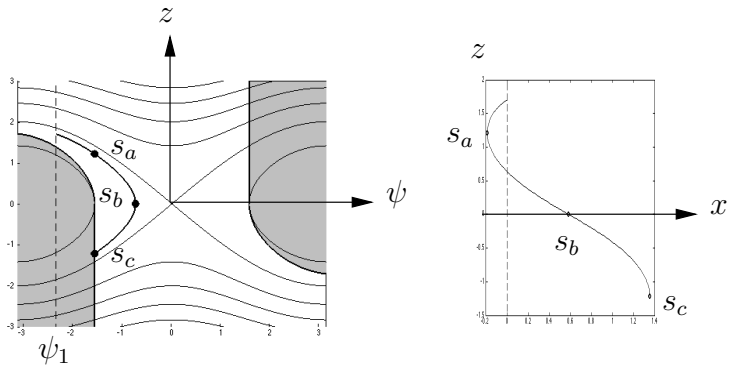

Figure 4: A solution which is a potential interface.

See Figure 4. For $0 \le s \le s_b$, we have $\dot{\psi} = \kappa z > 0$ and, integrating the first equation in (3), we find

$$x(s) = \int_{[0,s]} \cos\psi = \int_0^\psi \frac{\cos t}{\kappa z}\, dt.$$

Solving $\kappa z^2/2 + \cos\psi = h = \kappa\zeta^2/2 + \cos\theta$ for z, we find

$$x(s) = \frac{1}{\sqrt{2\kappa}} \int_\theta^\psi \frac{\cos t}{\sqrt{h - \cos t}}\, dt.$$

Extending the same reasoning beyond $s = s_b$, where ψ is decreasing with s, we obtain

$$\begin{aligned} x(s_c) &= \frac{1}{\sqrt{2\kappa}} \left[\int_\theta^{\psi_b} \frac{\cos t}{\sqrt{h - \cos t}}\, dt + \int_{-\pi/2}^{\psi_b} \frac{\cos t}{\sqrt{h - \cos t}}\, dt \right] \\ &= \frac{1}{\sqrt{2\kappa}} \left[\int_\theta^{-\pi/2} \frac{\cos t}{\sqrt{h - \cos t}}\, dt + 2\int_{-\pi/2}^{\psi_b} \frac{\cos t}{\sqrt{h - \cos t}}\, dt \right] \end{aligned} \tag{6}$$

where $\psi_b = \psi_{\max} \in (-\pi/2, 0)$ is determined by

$$\cos\psi_{\max} = h = \frac{\kappa\zeta^2}{2} + \cos\theta.$$

For reference, we observe that an integral of the form

$$I = \int_\psi^{\psi_{\max}} \frac{\cos t}{\sqrt{h - \cos t}}\, dt,$$

where $\cos\psi_{\max} = h$ as above, may be expressed as

$$I = -2\cot\psi\sqrt{h - \cos\psi} + 2\int_\psi^{\psi_{\max}} \csc^2 t\sqrt{h - \cos t}\, dt.$$

Consequently,

$$\frac{\partial I}{\partial \zeta} = -\kappa\zeta \left[\frac{\cot\psi}{\sqrt{h - \cos\psi}} + \int_\psi^{\psi_{\max}} \frac{\csc^2 t}{\sqrt{h - \cos t}}\, dt \right].$$

In particular,

$$\frac{\partial}{\partial\zeta} x(s_c) = \frac{\kappa\zeta}{\sqrt{2\kappa}} \left[-\frac{1}{2}\int_\theta^{-\pi/2} \frac{\cos t}{(h - \cos t)^{3/2}}\, dt + 4\int_{-\pi/2}^{\psi_b} \frac{\csc^2 t}{\sqrt{h - \cos t}}\, dt \right] > 0.$$

We are now in a position to state an initial exclusion result:

Theorem 2 *For each fixed $\theta \in [-\pi, -\pi/2)$, there is a unique $z_r > z_{\pi/2} > 0$ such that the solution of (3) with initial value $\zeta = z_r$ satisfies*

$$x(s_c; z_r) = 0.$$

Proof: Using expression (6) for $x(s_c)$, we find

$$\lim_{\zeta \searrow z_{\pi/2}} x(s_c; \zeta) = \frac{1}{\sqrt{2\kappa}} \int_\theta^{-\pi/2} \frac{\cos t}{\sqrt{h - \cos t}}\, dt < 0.$$

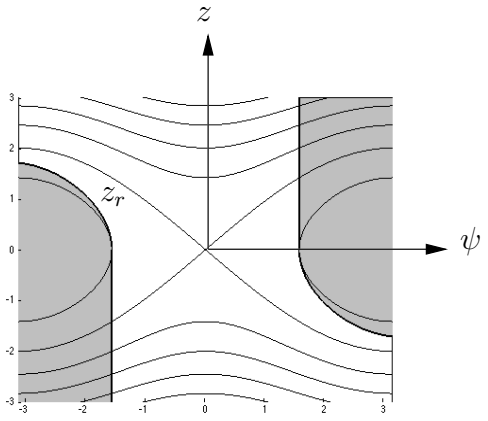

Figure 5: The phase plane showing z_r and the associated excluded regions.

On the other hand,

$$\lim_{\zeta \nearrow z_\infty} x(s_c;\zeta) = +\infty,$$

and the existence and uniqueness of z_r follows from the monotonicity of $x(s_c,\zeta)$ as a function of ζ. □

For solutions corresponding to $\zeta > z_\infty$, there are no inflections, but we obtain a second vertical point with

$$x = \frac{1}{\sqrt{2\kappa}} \int_\theta^{\pi/2} \frac{\cos t}{\sqrt{h - \cos t}}\, dt.$$

The monotonicity reverses with

$$\frac{\partial}{\partial \zeta} x = -\frac{\kappa\zeta}{2\sqrt{2\kappa}} \int_\theta^{\pi/2} \frac{\cos t}{(h - \cos t)^{3/2}}\, dt < 0,$$

and

$$\lim_{\zeta \searrow z_\infty} x = +\infty \qquad \text{with} \qquad \lim_{\zeta \nearrow +\infty} x = 0.$$

It is easy to check that all points in the strip $\{(\theta,\zeta) : -\pi/2 < \theta < \pi/2\}$ correspond to solutions in $\mathcal{S}_0$, and a symmetric situation prevails for $\pi/2 \le \theta \le \pi$. Consequently, we obtain the following.

Corollary 1 *The projection of $\mathcal{S}_0$ into the phase plane is precisely*

$$\{(\theta,\zeta) : -\pi/2 < \theta < \pi/2\} \cup \{(\theta,\zeta) : \pi/2 \le |\theta| \le \pi,\ \operatorname{sign}(\theta)\zeta < -z_r(-|\theta|)\}.$$

In particular, $\mathcal{S}_0$ is not empty.

The function $z_r = z_r(\theta)$ determines a positive, decreasing, concave graph on $[-\pi, -\pi/2]$ with $z_r(-\pi/2) = 0$ and $z_r(-\pi) \doteq 1.71019$ as indicated in Figure 5, though the only information needed for the discussion to follow is that $z_r \ge z_{\pi/2}$ with equality only for $\theta = -\pi/2$.

Corresponding to each point (θ, ζ) in the projection of $\mathcal{S}_0$ given in Corollary 1, the value

$$s_{\max} = s_{\max}(\theta, \zeta) = \sup\{s_* : (\theta, \zeta, s_*) \in \mathcal{S}_0\}$$

is a well-defined, positive extended real number. For example, if $-\pi \leq \theta \leq -\pi/2$ and $z_r < \zeta \leq z_\infty = \sqrt{2(1-\cos\theta)/2}$, then the situation of Figure 4 prevails with vertical points at $s = s_a$ and s_c and an inflection at $s = s_b$. It will be observed that $s_c = s_{\max}$ is the largest arclength s_* for which $(\theta, \zeta, s_*) \in \mathcal{S}_0$. In fact, if $s_* > s_c$, then condition 4 (that $\psi(s_*) \geq -\pi/2$) implies the parameterized orbit $(\psi(s), z(s))$ must complete an entire cycle in phase space. Let us denote the arclength of this cycle by $\bar{s}$. In particular, $\alpha(s_a + \bar{s})$ must be a vertical point in $\alpha[0, s_*]$. If $\alpha[0, s_*]$ is to be embedded in accord with condition 1, then $\alpha(s_a + \bar{s}) = \alpha(s_a) - \delta \mathbf{e}_1$ for some $\delta > 0$. That is, $\alpha(s_a + \bar{s})$ must be a left translation of $\alpha(s_a)$. But then $\alpha(s_*) = \alpha(s_* - \bar{s}) - \delta \mathbf{e}_1$ as well. Since $s_* - \bar{s} \geq s_a + \bar{s} - \bar{s} = s_a$, this means $\alpha(s_*)$ is also a left translation of another point in $\alpha[0, s_*]$. This violates condition 3 that $\alpha(s_*)$ must be the point farthest to the right.

Similar case by case considerations justify the following:

(i) Along the decreasing curve $\zeta = -\text{sign}(\theta) z_\infty = -\text{sign}(\theta)\sqrt{2(1-\cos\theta)/\kappa}$, solutions are portions of the singular solution[1] indicated in Figure 6. Consequently, $s_{\max} = +\infty$ and the maximum interval of definition is $[0, \infty)$.

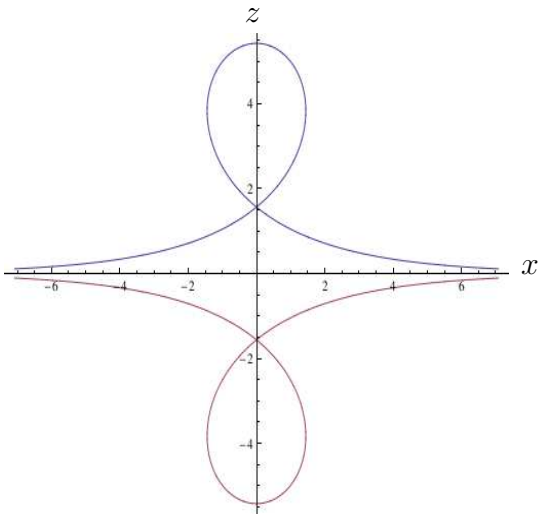

Figure 6: The soliton solution corresponding to $h = 1$.

(ii) If $\zeta \neq -\text{sign}(\theta) z_\infty$, then $s_{\max}$ is finite valued and determines a finite maximum interval of definition $[0, s_{\max}]$.

[1] Wente [Wen06, Wen11] (among others) refers to this as the soliton solution, but it is also known as the syntractrix of Poleni, who considered it in an equivalent form in 1729; see [Lev08]. Bhatnagar and Finn [BF06] also study this particular solution in the case of a laterally unbounded container.

(iii) If $\zeta < -\text{sign}(\theta) z_\infty$, then $\psi(s_{\max}) = -\pi/2$.

(iv) If $\zeta > -\text{sign}(\theta) z_\infty$, then $\psi(s_{\max}) = \pi/2$.

(v) One implication of conditions 1-4 is that for every solution in $\mathcal{S}_0$, we have

$$-\pi \le \psi(s) \le \pi, \quad 0 \le s \le s_*.$$

5 Secondary exclusions

In view of the monotonicity inequalities and limits of $x(s_*) = x(s_{\max})$ described in the previous section, we obtain the following result concerning the behavior of solutions corresponding to points in $\mathcal{S}_0$ at a fixed distance r to the right of the contact point.

Theorem 3 *For each $r > 0$, there are well defined finite values $\underline{z} < z_\infty < \bar{z}$ with $\underline{z} = \underline{z}(r) = \underline{z}(\theta, r)$ determined by the conditions*

$$x(s_{\max}(\underline{z}); \underline{z}) = r \quad \text{and} \quad \psi(s_{\max}(\underline{z}); \underline{z}) = -\pi/2,$$

and $\bar{z} = \bar{z}(r) = \bar{z}(\theta, r)$ determined by the conditions

$$x(s_{\max}(\bar{z}); \bar{z}) = r \quad \text{and} \quad \psi(s_{\max}(\bar{z}); \bar{z}) = \pi/2.$$

Furthermore, given θ and $r > 0$ fixed, the condition $x(s_{\max}; \zeta) \ge r$ holds precisely for $\underline{z} \le \zeta \le \bar{z}$.

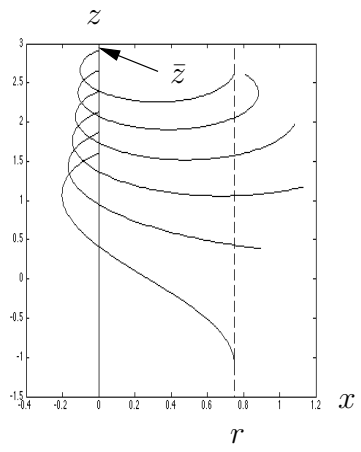

Figure 7: Monotonicity of ending contact angles and unique solution in $\mathcal{S}_2(r, \gamma_w)$ for a given θ and $r > 0$. The vertical dashed line represents $x = r$. The lowest solution starts at height $\underline{z}$, and the highest one starts at height $\bar{z}$.

In view of Theorem 3, which is illustrated in Figure 7, we set

$$\mathcal{S}_1(r) = \{(\theta, \zeta, s_*) \in \mathcal{S}_0 : \underline{z}(\theta, r) \le \zeta \le \bar{z}(\theta, r)\}.$$

Though we have not introduced the role of $\bar{\phi}$ and the other suppressed parameters explicitly, these results have obvious implications for condition 5. In particular, the following is now immediate from the properties of the inclination angle for solutions with $\underline{z} < \zeta < \bar{z}$:

Corollary 2 *For each $r > 0$, $\theta \in [-\pi/2, \pi/2]$, and $\zeta \in [\underline{z}(r), \bar{z}(r)]$, there is a unique $s_1 = s_1(\zeta) = s_1(\zeta; \theta, r) \leq s_{\max}(\zeta)$ for which*

$$x(s_1; \zeta) = r. \tag{7}$$

Notice that s_1 defines a particular ending arclength value for s_*. In particular, Conditions 1-7 may now be considered with $s_* = s_1$. It follows from Theorem 3 and continuity, that for any θ and r and any given angle $\psi_* \in [-\pi/2, \pi/2]$, there is at least one ζ between $\underline{z}$ and $\bar{z}$ for which $\psi(s_1(\zeta); \zeta) = \psi_*$. Note the implications of this assertion for Condition 6. Each point $(\theta, \zeta, s_1(\zeta))$ may be considered to correspond to a pseudo-equilibrium, though it may be that condition 7 is violated by such a configuration. See Figure 3(right). Uniqueness is not immediately obvious but follows from results in [McC15]. Numerically, the following stronger statement also implies uniqueness and stability for numerical calculations. This result is also illustrated in Figure 7.

Numerical result 1 *For θ and r fixed $s_1 = s_1(\zeta)$ determined by* (7)*,*

$$\frac{\partial}{\partial \zeta} \psi(s_1(\zeta); \zeta) > 0, \qquad \underline{z} < \zeta < \bar{z}.$$

Given the monotonicity implied by this result, or as found in [McC15], we have a unique value $z_1 = z_1(\theta, r)$ for which

$$\psi(s_1(z_1); \theta, z_1) = \frac{\pi}{2} - \gamma_w. \tag{8}$$

In the discussion above we have assumed r is fixed, and θ varies independently of $\bar{\phi}$. In the next section, we will have to take account of the fact that as $\bar{\phi}$ varies, the distance to be spanned satisfies $r = R - a\sin(\bar{\phi})$. In addition, we have the relation $\gamma - \theta = \bar{\phi}$. As a consequence, there is a choice of parameter in organizing the appropriate family of solutions. We may use as a single parameter either the azimuthal angle $\bar{\phi}$ or the initial inclination angle θ. The former has the advantage of having clear relevance to the contact point on the ball. The latter is convenient due to the role it plays in the phase diagram.

6 Secondary analysis of the geometry of solutions

We now address the additional conditions 5-7 in detail. Technically, this merely involves replacing r in the discussion above with the value $r = R - a\sin(\bar{\phi}) = R - a\sin(\gamma - \theta)$. Analytically, the ending arclength $s_* = s_1$ and the starting height $\zeta = z_1$ will be replaced with distinct alternatives. To be precise, we set

$$s_2(\zeta, \theta) = s_1(\zeta; \theta, R - a\sin(\gamma - \theta)) \quad \text{and} \quad z_G(\theta) = z_1(\theta, R - a\sin(\gamma - \theta)).$$

In addition, we define the one parameter family of *geometrically admissible solutions* by

$$\mathcal{S}_2 = \{(\theta, z_G(\theta), s_2(z_G(\theta), \theta)) \in \mathcal{S}_1 : -\pi \leq \theta \leq \pi\}.$$

In some cases, the graph of the function $z_G = z_G(\theta)$ in phase space may be plotted numerically as indicated in Figures 8, 9, and 10. In certain cases the qualitative behavior of z_G can be rigorously determined leading to conclusions about the collection of equilibria among the pseudo-equilibria. If it can be shown, for example, that z_G is decreasing, then there is a unique equilibrium. We will indicate how these conclusions can be obtained below.

Note that conditions 5 and 6 are automatically incorporated in $\mathcal{S}_2$. Condition 7 is somewhat more complicated and arises because we wish to avoid solutions which extend to the left past the

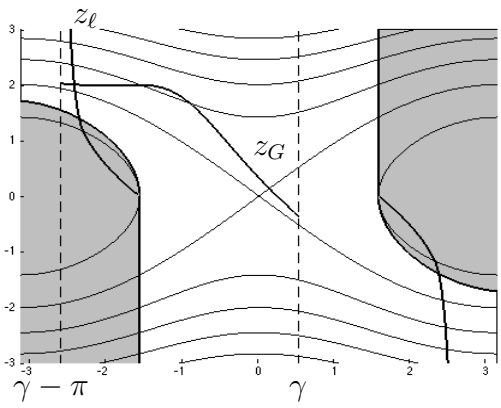

Figure 8: Restriction curves $\zeta = z_r$ and $\zeta = z_\ell$ and solution curve $\zeta = z_G$.

center of $\mathcal{B}$. Such solutions necessarily intersect the left component of $\mathcal{S}$ and lead to a nonphysical immersion as indicated in Figure 3(right).

In order to understand the restriction, it will be necessary to also impose the more restrictive condition on the beginning angle (5)

$$\gamma - \pi \leq \theta \leq \gamma$$

which may be easily incorporated in any of the solution sets $\mathcal{S}_j$ considered above or their projections into phase space. For example, this inequality is represented by the vertical dashed lines in Figure 8 where we have taken $\gamma = \pi/4$. Let us, therefore, denote the presence of these bounds on θ in $\mathcal{S}_j$ by $\bar{\mathcal{S}}_j$ for $j = 0, 1, 2$.

Then, in abstract terms, we can simply set

$$\mathcal{S}_3(a, R, \bar{\phi}, \gamma, \gamma_w) = \{(\theta, \zeta, s_2) \in \bar{\mathcal{S}}_2(R - a\sin\bar{\phi}, \gamma_w) : \ x(s) > -a\sin\bar{\phi}, \ s > 0\}.$$

For $\bar{\phi}$ very close to π which amounts to the same thing as θ being very close to the left boundary $\theta = \gamma - \bar{\phi}$, the condition determining the limits for this exclusion is

$$x(s_a; \zeta) = -a\sin\bar{\phi} \tag{9}$$

where s_a is the arclength corresponding to the first vertical point. Starting with $\theta < -\pi/2$ as usual, this first vertical point will be well defined for every solution under consideration and, in fact, the

corresponding $\zeta = z_\ell(\theta)$ tends to infinity as $\theta \searrow \gamma - \pi$ assuming, of course, that $\gamma - \pi < -\pi/2$. In the case we have described (9) becomes

$$\frac{1}{\sqrt{2\kappa}} \int_\theta^{-\pi/2} \frac{\cos t}{\sqrt{h - \cos t}}\, dt = -a \sin \bar{\phi},$$

and the monotonicity guarantees both the existence and uniqueness of a value $z_\ell = z_\ell(\theta)$ for which solutions with $\zeta \le z_\ell$ are inadmissible and solutions with $\zeta > z_\ell$ satisfy all geometric conditions of the problem. See Figure 8.

Numerical result 2 *If $\gamma < \pi/2$, there is a well-defined interval $\bar{\phi}_1 < \bar{\phi} < \pi$ such that for each $\theta \in (\gamma - \pi, \gamma - \bar{\phi}_1)$ there is a unique value $z = z_\ell(\theta)$, decreasing in θ and tending to infinity at the left such that*

$$\mathcal{S}_3(a, R, \bar{\phi}, \gamma, \gamma_w) \subset \{(\theta, \zeta, s_2) : z_\ell < \zeta\}.$$

If $\gamma > \pi/2$, this restriction on the basic condition $\zeta = z_G$ is vacuous on the left of the phase diagram where $\theta < -\pi/2$ but has a symmetric manifestation which will produce a nontrivial restriction for $\theta > \pi/2$. In the particular special case $\gamma = \pi/2$, these considerations concerning z_ℓ play no role at all. Typical behavior is indicated in Figure 8.

7 Force balance

Taking account of our remarks following (2) and noting that the curvature $\bar{k}$ is given in our translated coordinates simply by ζ, we obtain another fundamental condition on admissible equilibria:

Theorem 4 *Any equilibrium configuration must satisfy*

$$\zeta = z_F = \frac{\kappa a}{4 \sin \bar{\phi}} \left\{ 2\pi \left(1 - \frac{\rho}{\rho_\ell} \right) + \sin\left(2\bar{\phi}\right) - 2\bar{\phi} - \frac{4}{\kappa a^2} \sin\left(\bar{\phi} - \gamma\right) \right\} \tag{10}$$

which represents an increasing function of θ in the phase plane with

$$\lim_{\theta \searrow \gamma - \pi} z_F(\theta) = -\infty \qquad \text{and} \qquad \lim_{\theta \nearrow \gamma} z_F(\theta) = +\infty$$

as long as $0 \le \rho/\rho_\ell < 1$ and $0 < \gamma < \pi$.

Proof: Since $\theta = \gamma - \bar{\phi}$ it suffices to show

$$\frac{dz_F}{d\bar{\phi}} = \frac{1}{2a \sin^2 \bar{\phi}} \left\{ -2 \sin\gamma + \kappa a^2 \left[\bar{\phi} \cos\bar{\phi} - \sin\bar{\phi} \left(1 + \sin^2 \bar{\phi}\right) - \pi \left(1 - \frac{\rho}{\rho_\ell} \right) \cos\bar{\phi} \right] \right\}$$

is always negative. To see this, we consider

$$f(\bar{\phi}, P) = 2a \sin^2 \bar{\phi} \frac{dz_F}{d\bar{\phi}}$$

as a function of two variables on $[0, \pi] \times [0, 1]$ where $P = \rho/\rho_\ell$. Calculating the partial derivatives, we find

$$\frac{\partial f}{\partial P} = \kappa a^2 \pi \cos\bar{\phi}$$

and

$$\frac{\partial f}{\partial \bar{\phi}} = \kappa a^2 \left[\cos\bar{\phi} - \bar{\phi}\sin\bar{\phi} - \cos\bar{\phi}(1+\sin^2\bar{\phi}) - 2\sin^2\bar{\phi}\cos\bar{\phi} + \pi(1-P)\sin\bar{\phi}\right].$$

It follows that there is a unique interior critical point at $(\bar{\phi}, P) = (\pi/2, 1/2)$. The value at this point is

$$f(\pi/2, 1/2) = -2\sin\gamma - 2\kappa a^2 < 0.$$

Restricting the partial derivatives to the edges of the rectangle $[0,\pi]\times[0,1]$, we find all remaining extreme values must be in the corners. These values

$$\begin{aligned} f(\pi,0) &= -2\sin\gamma \\ f(0,0) &= -2\sin\gamma - \kappa a^2\pi \\ f(\pi,1) &= -2\sin\gamma - \kappa a^2\pi \\ f(0,1) &= -2\sin\gamma, \end{aligned}$$

are all strictly negative unless $\gamma = 0$ or $\gamma = \pi$. □

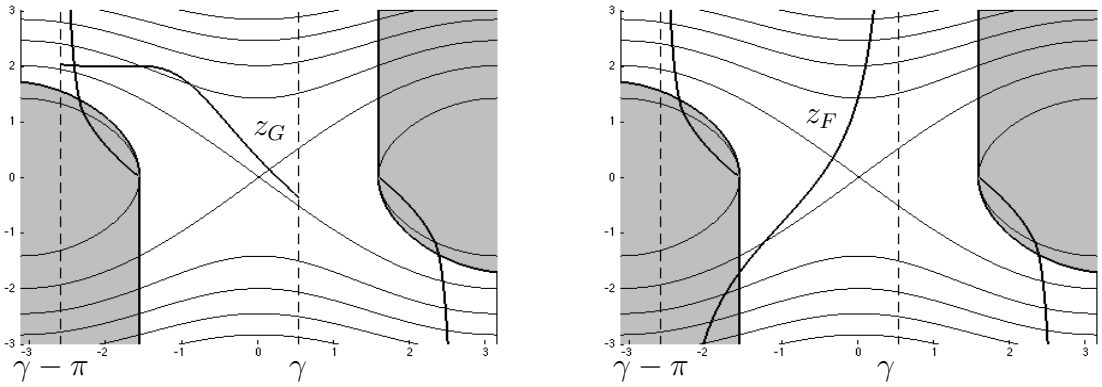

Figure 9: The geometric curve z_G and the force balance curve z_F in phase space.

Existence follows from the observation that when $\gamma \le \pi/2$

$$z_F(-\pi/2) < 0 \qquad \text{and} \qquad \lim_{\theta \nearrow \gamma} z_F(\theta) = +\infty,$$

and when $\gamma \ge \pi/2$

$$\lim_{\theta \searrow \gamma - \pi} z_F(\theta) = -\infty, \qquad \text{and} \qquad z_F(\pi/2) > 0.$$

Therefore the restrictions of z_r and z_ℓ on solutions (which only effect the region $\pi/2 < |\psi| < \pi$) cannot prevent the the graphs of z_G and z_F from intersecting in a point corresponding to an admissible equilibrium solution. See Figure 9. Thus we have proven Theorem 1.

This discussion has also the surprising corollary that there are no equilibrium interfaces which are essentially parametric. Intersection points between $-\pi/2$ and $\pi/2$ lead to equilibrium interfaces

that are graphs. The exclusions we have obtained force all the intersection points to be in this range. All equilibrium interfaces are graphs.

Theorem 5 *If $0 < \rho < \rho_\ell$ (and A large enough), there exists an equilibrium configuration satisfying the necessary conditions listed above. Additionally, all equilibrium interfaces are graphs.*

Finally, in many cases we have numerically verified that the "geometric curve" in phase space determined by $z_G = z_G(\theta)$ is decreasing. Combined with the proof that the "force balance curve" determined by $z_F = z_F(\theta)$ is increasing this implies that no more than one such solution may exist when $0 < \rho/\rho_\ell < 1$. However, the results in the next section show that this is not true in general. We leave the determination of precise physical conditions that lead to unique centrally located equilibria for another work.

8 An example of non uniqueness

Here we describe the main example. We assume homogeneous boundary conditions, that is, $\gamma = \gamma_w = \pi/2$. In this special case, condition 7 is never violated for $0 < \bar{\phi} < \pi$ and plays no essential role. We have the following system parametrized by arclength

$$\begin{cases} \dot{x} = \cos\psi, & x(0) = a\cos(\theta) \\ \dot{z} = \sin\psi, & u(0) = \zeta \\ \dot{\psi} = \kappa z, & \psi(0) = \theta. \end{cases} \tag{11}$$

When there are no inflection points along the profile curve this is equivalent to the following ODE parametrized by inclination angle

$$\begin{cases} \frac{dx}{d\psi} & = \frac{-\cos\psi}{\sqrt{\zeta^2+2(\cos\theta-\cos\psi)}} \\ x(\theta) & = a\cos\theta, \end{cases} \tag{12}$$

for ψ starting at θ and decreasing to 0. This fact follows from the conserved quantity

$$\frac{1}{2}z^2 + \cos\psi = q = \frac{1}{2}\zeta^2 + \cos\theta, \tag{13}$$

which implies

$$z = -\sqrt{\zeta^2 + 2(\cos\theta - \cos\psi)}. \tag{14}$$

We have taken this sign convention as the equilibria obtained below have negative interface height.

Next, we prescribe the container width of $2R$, with $R = 4$, and we choose a ball with radius 99.9% of R, or $a = 3.996$. For each $\theta \in (0, \pi/2)$ we solve the boundary value problem of determining a value of ζ in (12) so that $x(0) = R$. We employ a shooting method and provide an initial guess of $-1.2\sqrt{2(1-\cos(\theta))}$, which is a scaled value of the height of the soliton solution at that θ. With this starting guess, we use a zero finding algorithm implemented as fzero in Matlab to determine $\zeta = z_G = z_G(\theta)$ that achieves the condition $x(0) = R$ within tolerance.

Next, we compute

$$\zeta = z_F = \frac{\kappa a}{4\sin\bar{\phi}}\left\{2\pi\left(1 - \frac{\rho}{\rho_\ell}\right) + \sin\left(2\bar{\phi}\right) - 2\bar{\phi} - \frac{4}{\kappa a^2}\sin\left(\bar{\phi} - \gamma\right)\right\} \tag{15}$$

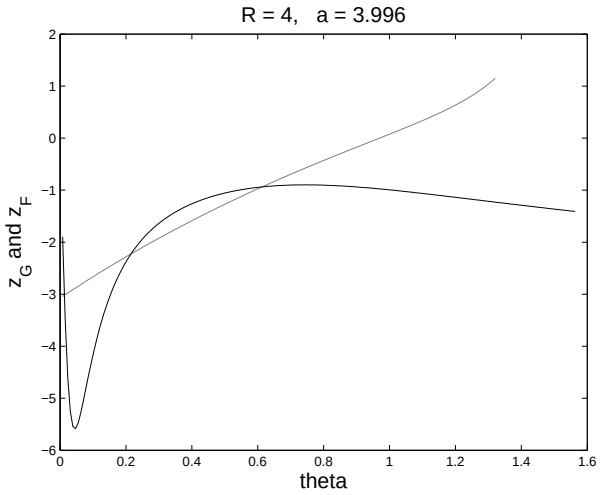

Figure 10: Graphs of z_G and z_F.

using the fact that $\bar{\phi} = \pi/2 - \theta$. Here we are able to adjust the density ratio for particular examples, and we choose $\rho/\rho_\ell = 0.99$.

Finally, we graph both $z_G(\theta)$ and $z_F(\theta)$, looking for intersections of the graphs. See Figure 10. Notice there are three intersections. We use a grid with 200 values of θ and cycle through the data. Upon finding a sign change, we used the secant method to locate the zero of $(z_G - z_F)(\theta)$. Of course, much more sophisticated methods could easily be employed if more accurate values were desired. We have located three distinct equilibria for the centrally located floating ball with these physical parameters, and thus there is no uniqueness in this case.

In Figures 11-13 we show the right half of the symmetric configurations generated by these distinct θ values. The two equilibria corresponding to azimuthal angle $\bar{\phi}$ slightly less than $\pi/2$ look relatively similar from a distance. With magnification around the interface, however, the difference is clearly seen, as shown in Figures 12-13.

Technically the methods we have used here do not indicate if these equilibria are local minima, maxima, saddle points, or even stable or unstable. Nevertheless, the energy of pseudo-equilibria can be computed and compared as well as the relative energies of actual equilibria. Thus, when we refer to a *local energy minimum or maximum,* we mean with respect to pseudo-equilibria. In this case, the energies of the pseudo-equilibria (one parameter family) are plotted in Figure 14, and we see that two of the equilibria are local energy minima among pseudo-equilibria and the third is a local max. Also, we can say that the equilibrium with the azimuthal angle closest to $\pi/2$ has the least possible energy for an equilibrium and is the presumed global energy minimizer for the problem.

The really interesting possibility, however, is that it may be the case that the other local energy minimizer among pseudo-equilibria may actually be a local energy minimizer among all configurations and, thus, may be observable in a physical system. Let's call this the "large" interface. There is also a possibility that there is a lower energy path of configurations connecting the large interface

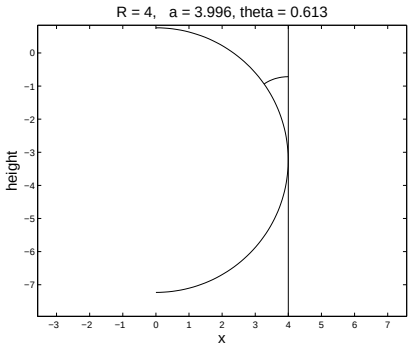

Figure 11: The configuration with $\theta = 0.613$. This "large" inteface yields a local minimum, but has higher energy than one of the other equilibria.

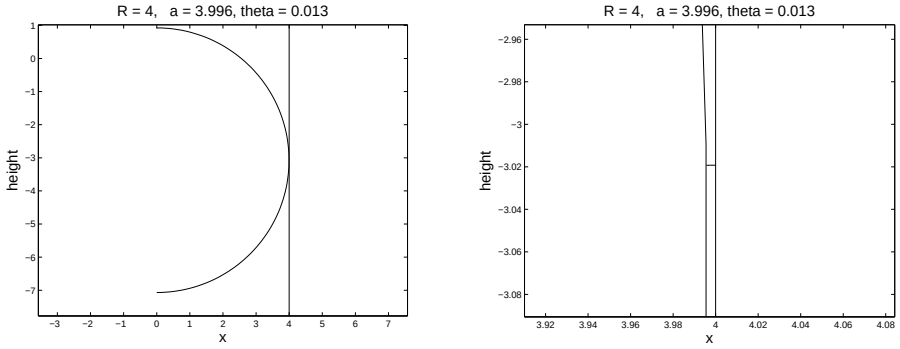

Figure 12: The configuration with $\theta = 0.013$, with a detailed zoom on the right. This is a local minimum, and has the lowest possible energy of any centrally located equilibrium.

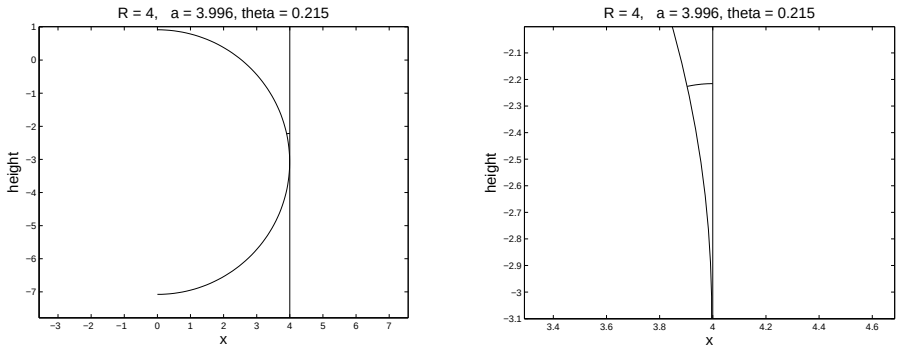

Figure 13: The configuration with $\theta = 0.215$, with a detailed zoom on the right. This is a local maximum of energy.

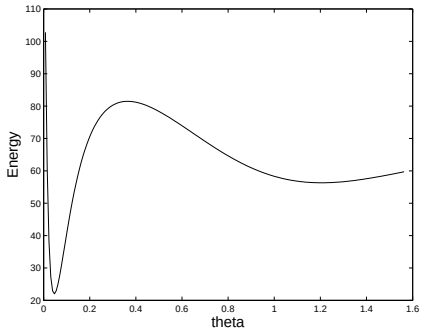

Figure 14: The energy as a function of θ.

to the global min. Such a path does not exist among pseudo-equilibria.

References

[BF06] R. Bhatnagar and R. Finn. Equilibrium configurations of an infinite cylinder in an unbounded fluid. *Phys. Fluids*, 18(4):047103, 7, 2006.

[Che16] H. Chen. Floating bodies with surface tension. Master's thesis, University of Waterloo, 2016.

[Fin08] R. Finn. The floating ball "paradox". *Journal of Mathematical Fluid Mechanics*, 10:583–587, 2008.

[Fin09] R. Finn. Floating bodies subject to capillary attractions. *Journal of Mathematical Fluid Mechanics*, 11:443–458, 2009.

[Fin10] R. Finn. On Young's paradox, and the attractions of immersed parallel plates. *Physics of Fluids*, 22(017103), 2010.

[Fin11] R. Finn. Criteria for floating I. *Journal of Mathematical Fluid Mechanics*, 13:103–115, 2011.

[FS09] R. Finn and M. Sloss. Floating bodies in neutral equilibrium. *Journal of Mathematical Fluid Mechanics*, 11:459–463, 2009.

[FV09a] R. Finn and T. Vogel. Floating criteria in three dimensions. *Analysis (Munich)*, 29:125–140, 2009.

[FV09b] R. Finn and T. Vogel. Floating criteria in three dimensions. *Analysis (Munich)*, 29:387–402, 2009.

[KS11] T. Kemp and D. Siegel. Floating bodies in two dimensions without gravity. *Ph. of Fluids*, 23, 2011.

[Lev08] R. Levien. The elastica: a mathematical history. Technical Report UCB/EECS-2008-103, EECS Department, University of California, Berkeley, Aug 2008.

[McC07] J. McCuan. A variational formula for floating bodies. *Pac. J. Math.*, 231:167–191, 2007.

[McC09] John McCuan. Archimedes revisited. *Milan J. Math.*, 77:385–396, 2009.

[McC15] J. McCuan. New geometric estimates for euler elastica. *JEPE*, 1:387–402, 2015.

[MT13] J. McCuan and R. Treinen. Capillarity and Archimedes' principle of flotation. *Pac. J. Math.*, 265:123–150, 2013.

[Tre16] R. Treinen. Examples of non-uniqueness of the equilibrium states for a floating ball. *Adv. Materials Phys. Chem.*, 6:177–194, 2016.

[Wen06] H. Wente. New exotic containers. *Pac. J. Math.*, 224:379–398, 2006.

[Wen11] H. Wente. Exotic capillary tubes. *J. Math.Fluid Mech*, 13:355–370, 2011.